Equivariant IMU Preintegration with Biases: an Inhomogeneous Galilean Group Approach

Giulio Delama[1*], Alessandro Fornasier[1*] and Stephan Weiss[1]

***Abstract*—This paper proposes a new approach for Inertial Measurement Unit (IMU) preintegration, a fundamental building block that can be leveraged in different optimization-based Inertial Navigation System (INS) localization solutions. Inspired by recent advancements in equivariant theory applied to biased INSs, we derive a discrete-time formulation of the IMU preintegration on $\mathbf{G}(3) \ltimes \mathfrak{g}(3)$, the tangent group of the inhomogeneous Galilean group $\mathbf{G}(3)$. We define a novel preintegration error that geometrically couples the navigation states and the bias leading to lower linearization error. Our method improves in consistency compared to existing preintegration approaches which treat IMU biases as a separate state-space.**

I. Introduction and Related Work

Inertial Navigation Systems stand out as localization methods for their ability to utilize data from IMUs and fuse it with other sensors to determine the position and orientation of a mobile robot. However, traditional INS approaches often encounter challenges related to biases in the IMU measurements, yielding decreased performances in real-world applications. The recent introduction of the *equivariant* filter (EqF) [1]–[3] has shown significant improvement in state estimation for biased INSs [3], [4]. Researchers have successfully improved consistency, robustness, and accuracy by leveraging *bias-inclusive* symmetries and developing EqFs [3]–[11] that outperform state-of-the-art methods based on the classical Extended Kalman Filter (EKF) and Invariant Extended Kalman Filter (IEKF) [12]. Despite the advancements in the EqF domain, a crucial gap persists in applying this novel and promising theory to optimization-based estimation techniques, whose increasing traction is driven by the growing affordability of powerful and compact computing boards.

In the attempt to take a first step in that direction, this work focuses on the *IMU preintegration* problem. IMU preintegration has become an essential component of optimization-based localization methods for INSs since it allows the formulation of a factor between two non-consecutive IMU poses by exclusively relying on inertial measurements.

To the best of the authors' knowledge, previous research on IMU preintegration [13]–[19] has not exploited the symmetry of the system to formulate an error that geometrically couples the navigation and the bias states, instead of treating them separately. This paper presents a novel equivariant approach to the IMU preintegration problem. We introduce a symmetry based on the tangent group of the *inhomogeneous Galilean group* $\mathbf{G}(3) \ltimes \mathfrak{g}(3)$ and we define a linearized error dynamics based on the *equivariant error*, which effectively establishes a geometric coupling between the navigation states and the bias states, thus resulting in *better linearization* for the navigation states' error. We extensively tested our novel *equivariant* IMU preintegration: our method exhibited superior performance in terms of consistency compared to state-of-the-art preintegration methods [13], [16]–[18] in all the sequences of the well-known EuRoC MAV dataset [20].

[1]Giulio Delama, Alessandro Fornasier, and Stephan Weiss are with the Control of Networked Systems Group, University of Klagenfurt, Austria. * G. Delama and A. Fornasier contributed equally. {giulio.delama, alessandro.fornasier, stephan.weiss}@ieee.org

Algorithm 1 IMU Preintegration on $\mathbf{G}(3) \ltimes \mathfrak{g}(3)$

Define: $\mathring{\xi} = (\mathbf{I}_5,\ \mathbf{0}_{10\times1})$, $\hat{X}_0 = (\mathbf{I}_5,\ -\boldsymbol{b}_0^\wedge)$, $\mathbf{J}_{\xi_0} = \mathbf{I}_{20}$, $\boldsymbol{\Sigma}_0$, $\mathbf{Q}_\mathbf{d} = \mathrm{diag}(\boldsymbol{\sigma}_{d\omega}^2,\ \boldsymbol{\sigma}_{da}^2,\ \mathbf{0}_{4\times1},\ \boldsymbol{\sigma}_{d\tau_\omega}^2,\ \boldsymbol{\sigma}_{d\tau_a}^2,\ \mathbf{0}_{4\times1})$.
Input: $\tilde{\boldsymbol{w}}_k = (\tilde{\boldsymbol{\omega}}_k,\ \tilde{\boldsymbol{a}}_k,\ \mathbf{0}_{3\times1},\ 1)$, $\boldsymbol{\tau}_k = \mathbf{0}_{10\times1}$, $\delta t = t_{k+1} - t_k$.
Output: $\hat{X}_{k+1} \Leftrightarrow \hat{\xi}_{k+1}$, $\boldsymbol{\Sigma}_{k+1}$, $\mathbf{J}_{\xi_{k+1}}$.

Require: IMU measurements $(\tilde{\boldsymbol{\omega}}_k,\ \tilde{\boldsymbol{a}}_k)$ from $k = 0$ to N
for $k \leftarrow 0$ to N **do**
$\tilde{u}_k \leftarrow (\tilde{\boldsymbol{w}}_k,\ \tilde{\boldsymbol{\tau}}_k)$
$\hat{X}_{k+1} \leftarrow \hat{X}_k \Lambda_{\delta t}(\phi_{\mathring{\xi}}(\hat{X}_k), \tilde{u}_k)$ (23)
$\hat{\xi}_{k+1} \leftarrow \phi_{\mathring{\xi}}(\hat{X}_{k+1})$ (28)
$\boldsymbol{\Sigma}_{k+1} \leftarrow \hat{\mathbf{A}}_{k+1}\boldsymbol{\Sigma}_k\hat{\mathbf{A}}_{k+1}^\top + \hat{\mathbf{B}}_{k+1}\mathbf{Q}_\mathbf{d}\hat{\mathbf{B}}_{k+1}^\top$ (30)
$\mathbf{J}_{\xi_{k+1}} \leftarrow \boldsymbol{\Phi}_{\mathbf{b}k+1}\mathbf{J}_{\xi_k}$ (33)
end for

II. The Inhomogeneous Galilean Group

Let $X \in \mathbf{G}(3)$ denote an element of the inhomogeneous Galilean group, represented in its matrix form as

$$\mathbf{X} = \begin{bmatrix} \mathbf{A} & \boldsymbol{a} & \boldsymbol{b} \\ \mathbf{0}_{1\times3} & 1 & c \\ \mathbf{0}_{1\times3} & 0 & 1 \end{bmatrix} \in \mathbb{R}^{5\times5}, \tag{1}$$

with $\mathbf{A} \in \mathbf{SO}(3)$, $\boldsymbol{a}$, $\boldsymbol{b} \in \mathbb{R}^3$ and $c \in \mathbb{R}$.
Let $\boldsymbol{x} \in \mathbb{R}^{10}$ so that $\boldsymbol{x}^\wedge \in \mathfrak{g}(3)$ denote an element of the Lie algebra of $\mathbf{G}(3)$, which is represented by the matrix form

$$\boldsymbol{x}^\wedge = \begin{bmatrix} \boldsymbol{\omega} \\ \boldsymbol{v} \\ \boldsymbol{w} \\ \alpha \end{bmatrix}^\wedge = \begin{bmatrix} \boldsymbol{\omega}^\wedge & \boldsymbol{v} & \boldsymbol{w} \\ \mathbf{0}_{1\times3} & 0 & \alpha \\ \mathbf{0}_{1\times3} & 0 & 0 \end{bmatrix} \in \mathbb{R}^{5\times5}, \tag{2}$$

with $\boldsymbol{\omega}^\wedge \in \mathbf{SO}(3)$, $\boldsymbol{v}, \boldsymbol{w} \in \mathbb{R}^3$ and $\alpha \in \mathbb{R}$.
The inverse element in matrix form is written

$$\mathbf{X}^{-1} = \begin{bmatrix} \mathbf{A}^\top & -\mathbf{A}^\top\boldsymbol{a} & -\mathbf{A}^\top(\boldsymbol{b} - c\,\boldsymbol{a}) \\ \mathbf{0}_{1\times3} & 1 & -c \\ \mathbf{0}_{1\times3} & 0 & 1 \end{bmatrix} \in \mathbb{R}^{5\times5}. \tag{3}$$

The adjoint matrices are defined as

$$\mathbf{Ad}_{\mathbf{X}}^{\vee} \coloneqq \begin{bmatrix} \mathbf{A} & \mathbf{0}_{3\times3} & \mathbf{0}_{3\times3} & \mathbf{0}_{3\times1} \\ \boldsymbol{a}^{\wedge}\mathbf{A} & \mathbf{A} & \mathbf{0}_{3\times3} & \mathbf{0}_{3\times1} \\ (\boldsymbol{b}-c\,\boldsymbol{a})^{\wedge}\mathbf{A} & -c\mathbf{A} & \mathbf{A} & \boldsymbol{a} \\ \mathbf{0}_{1\times3} & \mathbf{0}_{1\times3} & \mathbf{0}_{1\times3} & 1 \end{bmatrix}, \tag{4}$$

$$\mathbf{ad}_{\boldsymbol{x}}^{\vee} \coloneqq \begin{bmatrix} \boldsymbol{\omega}^{\wedge} & \mathbf{0}_{3\times3} & \mathbf{0}_{3\times3} & \mathbf{0}_{3\times1} \\ \boldsymbol{v}^{\wedge} & \boldsymbol{\omega}^{\wedge} & \mathbf{0}_{3\times3} & \mathbf{0}_{3\times1} \\ \boldsymbol{w}^{\wedge} & -\alpha\mathbf{I}_3 & \boldsymbol{\omega}^{\wedge} & \boldsymbol{v} \\ \mathbf{0}_{1\times3} & \mathbf{0}_{1\times3} & \mathbf{0}_{1\times3} & 0 \end{bmatrix}. \tag{5}$$

Closed forms of the exponential and logarithmic maps are

$$\exp(\boldsymbol{x}^{\wedge}) = \begin{bmatrix} \exp(\boldsymbol{\omega}^{\wedge}) & \boldsymbol{\Gamma}_1(\boldsymbol{\omega})\boldsymbol{v} & \boldsymbol{\Gamma}_1(\boldsymbol{\omega})\boldsymbol{w}+\alpha\boldsymbol{\Gamma}_2(\boldsymbol{\omega})\boldsymbol{v} \\ \mathbf{0}_{1\times3} & 1 & \alpha \\ \mathbf{0}_{1\times3} & 0 & 1 \end{bmatrix}, \tag{6}$$

$$\log(X) = \begin{bmatrix} \log(\mathbf{A}) & \boldsymbol{\Gamma}_1(\log(\mathbf{A})^{\vee})^{-1}\boldsymbol{a} & \boldsymbol{\Gamma}_1(\log(\mathbf{A})^{\vee})^{-1}\boldsymbol{\Xi} \\ \mathbf{0}_{1\times3} & 0 & c \\ \mathbf{0}_{1\times3} & 0 & 0 \end{bmatrix}, \tag{7}$$

with $\boldsymbol{\Xi} = \big(\boldsymbol{b} - c\boldsymbol{\Gamma}_2(\log(\mathbf{A})^{\vee})\boldsymbol{\Gamma}_1(\log(\mathbf{A})^{\vee})^{-1}\,\boldsymbol{a}\big)$.
$\boldsymbol{\Gamma}_1$ and $\boldsymbol{\Gamma}_2$ denote respectively the $\mathbf{SO}(3)$ left Jacobian and auxiliary function [21], both with known closed-form expressions $\boldsymbol{\Gamma}_1(\boldsymbol{\omega}) = \mathbf{I}_3 + \kappa_1\,\boldsymbol{\omega}^{\wedge} + \kappa_2\,\boldsymbol{\omega}^{\wedge}\boldsymbol{\omega}^{\wedge}$ and $\boldsymbol{\Gamma}_2(\boldsymbol{\omega}) = \frac{1}{2}\mathbf{I}_3 + \kappa_2\,\boldsymbol{\omega}^{\wedge} + \kappa_3\,\boldsymbol{\omega}^{\wedge}\boldsymbol{\omega}^{\wedge}$ with $\kappa_1 = \frac{1-\cos(\|\boldsymbol{\omega}\|)}{\|\boldsymbol{\omega}\|^2}$, $\kappa_2 = \frac{\|\boldsymbol{\omega}\|-\sin(\|\boldsymbol{\omega}\|)}{\|\boldsymbol{\omega}\|^3}$, and $\kappa_3 = \frac{\|\boldsymbol{\omega}\|^2+2\cos(\|\boldsymbol{\omega}\|-2)}{2\|\boldsymbol{\omega}\|^4}$.
Finally, the closed-form of the $\mathbf{G}(3)$ left Jacobian $\mathbf{J}_{\mathrm{L}}$ is

$$\mathbf{J}_{\mathrm{L}}(\boldsymbol{x}) = \begin{bmatrix} \boldsymbol{\Gamma}_1(\boldsymbol{\omega}) & \mathbf{0}_{3\times3} & \mathbf{0}_{3\times3} & \mathbf{0}_{3\times1} \\ \mathbf{Q}_1(\boldsymbol{\omega},\boldsymbol{v}) & \boldsymbol{\Gamma}_1(\boldsymbol{\omega}) & \mathbf{0}_{3\times3} & \mathbf{0}_{3\times1} \\ \boldsymbol{\Omega} & -\alpha\mathbf{U}_1(\boldsymbol{\omega}) & \boldsymbol{\Gamma}_1(\boldsymbol{\omega}) & \boldsymbol{\Gamma}_2(\boldsymbol{\omega})\,\boldsymbol{v} \\ \mathbf{0}_{1\times3} & \mathbf{0}_{1\times3} & \mathbf{0}_{1\times3} & 1 \end{bmatrix}, \tag{8}$$

with $\boldsymbol{\Omega} = \mathbf{Q}_1(\boldsymbol{\omega},\boldsymbol{w}) - \alpha\mathbf{Q}_2(\boldsymbol{\omega},\boldsymbol{v})$.

The closed-form expressions for $\mathbf{Q}_1$, $\mathbf{Q}_2$, and $\mathbf{U}_1$ have been omitted for space limitations[1].

III. Equivariant IMU preintegration

The core contribution of this work is the derivation of a novel *discrete-time* formulation for the *equivariant* IMU preintegration on the tangent group of $\mathbf{G}(3)$, i.e., $\mathbf{G}(3) \ltimes \mathfrak{g}(3)$.

A. Biased Inertial Navigation System (INS)

Consider a mobile robot equipped with an IMU that delivers biased angular velocity and acceleration measurements. Under non-rotating, flat earth assumption, the noise-free continuous-time biased INS is characterized by the following equations:

$$\dot{\mathbf{R}} = \mathbf{R}\,(\boldsymbol{\omega} - \boldsymbol{b}_{\omega})^{\wedge}, \tag{9a}$$
$$\dot{\boldsymbol{v}} = \mathbf{R}\,(\boldsymbol{a} - \boldsymbol{b}_a) + \boldsymbol{g}, \tag{9b}$$
$$\dot{\boldsymbol{p}} = \boldsymbol{v}, \tag{9c}$$
$$\dot{\boldsymbol{b}}_{\omega} = \boldsymbol{\tau}_{\omega}, \tag{9d}$$
$$\dot{\boldsymbol{b}}_a = \boldsymbol{\tau}_a, \tag{9e}$$

where $\mathbf{R} \in \mathbf{SO}(3)$ and $\boldsymbol{v}, \boldsymbol{p} \in \mathbb{R}^3$ denote the *core states* (or *navigation states*), i.e., the rigid body orientation, velocity, and position in the global reference frame. $\boldsymbol{b}_{\omega}, \boldsymbol{b}_a \in \mathbb{R}^3$ denote the *bias state*, $\boldsymbol{g} \in \mathbb{R}^3$ is the gravity vector, and $\boldsymbol{\omega}, \boldsymbol{a} \in \mathbb{R}^3$ are the *biased* rigid body angular velocity and acceleration. $\boldsymbol{\tau}_{\omega}, \boldsymbol{\tau}_a \in \mathbb{R}^3$ are inputs used to model the evolution of the bias terms, e.g., they are zero if the biases are modeled as constant quantities. Similarly to [3], [4], by extending (9) with additional virtual inputs and bias states, the noise-free biased INS can be reformulated as follows.

Let $\xi = (\mathbf{T},\, \boldsymbol{b}) \in \mathcal{M} \coloneqq \mathcal{SE}_2(3) \times \mathbb{R}^9$ represent the state of the augmented system, where the extended pose $\mathbf{T} = (\mathbf{R},\, \boldsymbol{v},\, \boldsymbol{p}) \in \mathcal{SE}_2(3)$ represents the core states and $\boldsymbol{b} = (\boldsymbol{b}_{\omega},\, \boldsymbol{b}_a,\, \boldsymbol{b}_{\nu}) \in \mathbb{R}^9$ represents the bias states, including the IMU biases and an additional virtual velocity bias $\boldsymbol{b}_{\nu} \in \mathbb{R}^3$, which was initially introduced in [3]. Define the systems' input $u = (\boldsymbol{w},\, \boldsymbol{\tau}) \in \mathbb{L} \subseteq \mathbb{R}^{18}$, where $\boldsymbol{w} = (\boldsymbol{\omega},\, \boldsymbol{a},\, \boldsymbol{\nu}) \in \mathbb{R}^9$ includes the inertial measurements and an additional virtual velocity input $\boldsymbol{\nu} = \mathbf{0}_{3\times1}$, and $\boldsymbol{\tau} = (\boldsymbol{\tau}_{\omega},\, \boldsymbol{\tau}_a,\, \boldsymbol{\tau}_{\nu}) \in \mathbb{R}^9$ denotes the biases input. By defining the matrices

$$\mathbf{G} \coloneqq \begin{bmatrix} \mathbf{0}_{3\times3} & \boldsymbol{g} & \mathbf{0}_{3\times1} \\ \mathbf{0}_{2\times3} & \mathbf{0}_{2\times1} & \mathbf{0}_{2\times1} \end{bmatrix} \in \mathbb{R}^{5\times5}, \quad \mathbf{N} \coloneqq \begin{bmatrix} \mathbf{0}_{3\times4} & \mathbf{0}_{3\times1} \\ \mathbf{0}_{1\times4} & 1 \\ \mathbf{0}_{1\times4} & 0 \end{bmatrix} \in \mathbb{R}^{5\times5},$$

we can represent the noise-free continuous-time biased INS in compact form as $\dot{\xi} = f(\xi, u)$, that is

$$\begin{cases} \dot{\mathbf{T}} = (\mathbf{G} - \mathbf{N})\,\mathbf{T} + \mathbf{T}(\boldsymbol{w}^{\wedge} - \boldsymbol{b}^{\wedge} + \mathbf{N}) \\ \dot{\boldsymbol{b}} = \boldsymbol{\tau} \end{cases}, \tag{10}$$

where $\boldsymbol{w}^{\wedge}, \boldsymbol{b}^{\wedge} \in \mathfrak{se}_2(3)$.

B. Discrete-time IMU preintegration

Under the assumption of a constant noise-free input u_i between consecutive time steps t_i and t_{i+1}, the exact discretization of (10) results in the following discrete-time formulation of the noise-free biased INS:

$$\begin{cases} \mathbf{T}_{i+1} = \exp\big((\mathbf{G} - \mathbf{N})\delta t\big)\,\mathbf{T}_i \exp\big((\boldsymbol{w}_i^{\wedge} - \boldsymbol{b}_i^{\wedge} + \mathbf{N})\delta t\big) \\ \boldsymbol{b}_{i+1} = \boldsymbol{b}_i + \boldsymbol{\tau}_i \delta t \end{cases}, \tag{11}$$

where $\xi_i = (\mathbf{T}_i,\, \boldsymbol{b}_i)$ and $u_i = (\boldsymbol{w}_i,\, \boldsymbol{\tau}_i)$ denote the state and the input at the i-th time step, and $\delta t = t_{i+1} - t_i$. Here, $\exp(\cdot)$ denotes the matrix exponential. Given two non-consecutive time steps t_i and t_j, and defining the *preintegration time* $\Delta t_{ij} = t_j - t_i$, the newest pose $\mathbf{T}_j$ is given by

$$\mathbf{T}_j = \boldsymbol{\Gamma}_{ij}\,\mathbf{T}_i\boldsymbol{\Upsilon}_{ij}, \tag{12}$$

where $\boldsymbol{\Gamma}_{ij}$ and $\boldsymbol{\Upsilon}_{ij}$ are exact integration terms defined as

$$\boldsymbol{\Gamma}_{ij} \coloneqq \prod_{k=i}^{j-1} \exp\big((\mathbf{G} - \mathbf{N})\delta t\big) = \begin{bmatrix} \mathbf{I}_3 & \boldsymbol{g}\Delta t_{ij} & -\frac{1}{2}\boldsymbol{g}\Delta t_{ij}^2 \\ \mathbf{0}_{1\times3} & 1 & -\Delta t_{ij} \\ \mathbf{0}_{1\times3} & 0 & 1 \end{bmatrix}, \tag{13}$$

$$\boldsymbol{\Upsilon}_{ij} \coloneqq \prod_{k=i}^{j-1} \exp\big((\boldsymbol{w}_k^{\wedge} - \boldsymbol{b}_k^{\wedge} + \mathbf{N})\delta t\big) = \begin{bmatrix} \Delta\mathbf{R}_{ij} & \Delta\boldsymbol{v}_{ij} & \Delta\boldsymbol{p}_{ij} \\ \mathbf{0}_{1\times3} & 1 & \Delta t_{ij} \\ \mathbf{0}_{1\times3} & 0 & 1 \end{bmatrix}. \tag{14}$$

Note that $\boldsymbol{\Gamma}_{ij}$ is not to be confused with $\boldsymbol{\Gamma}_1$ and $\boldsymbol{\Gamma}_2$ of Sec. II. By reorganizing (12) we obtain the following expression:

$$\boldsymbol{\Upsilon}_{ij} = \mathbf{T}_i^{-1}\boldsymbol{\Gamma}_{ij}^{-1}\,\mathbf{T}_j. \tag{15}$$

We refer to $\boldsymbol{\Upsilon}_{ij}$ as the *preintegration matrix*, which stores all the necessary information for relating $\mathbf{T}_j$ with $\mathbf{T}_i$, as outlined in (15). By reworking (14), the iterative computation of the preintegration matrix, starting from $j = i$ with $\boldsymbol{\Upsilon}_{ii} = \mathbf{I}_5$, is

$$\boldsymbol{\Upsilon}_{i(j+1)} = \boldsymbol{\Upsilon}_{ij} \exp\big((\boldsymbol{w}_j^{\wedge} - \boldsymbol{b}_j^{\wedge} + \mathbf{N})\delta t\big). \tag{16}$$

[1]For the interested reader: https://seafile.aau.at/d/42179d0d19d14f3c9e67/

C. Symmetry of the preintegration problem

Equation (14) reveals that the preintegration matrix can be represented as an element of the inhomogeneous Galilean group $\mathbf{G}(3)$, which has been formalized in Sec. II. From here onward, we adopt a lean notation by defining $\boldsymbol{\Upsilon}_k \coloneqq \boldsymbol{\Upsilon}_{i(i+k)}$ and $\boldsymbol{b}_k \coloneqq \boldsymbol{b}_{i+k}$, with $\xi_0 = (\boldsymbol{\Upsilon}_0,\ \boldsymbol{b}_0) = (\mathbf{I}_5,\ \boldsymbol{b}_i)$.

Let us define $\mathcal{M} \coloneqq \mathcal{G}(3) \times \mathbb{R}^{10}$ and let $\xi_k = (\boldsymbol{\Upsilon}_k,\ \boldsymbol{b}_k) \in \mathcal{M}$ represent the state of our system. The preintegration matrix $\boldsymbol{\Upsilon}_k = (\Delta\mathbf{R}_k,\ \Delta\boldsymbol{v}_k,\ \Delta\boldsymbol{p}_k,\ \Delta t_k) \in \mathcal{G}(3)$ denotes the preintegrated navigation states and the preintegration time. The bias states are denoted by $\boldsymbol{b}_k = (\boldsymbol{b}_{\omega k},\ \boldsymbol{b}_{ak},\ \boldsymbol{b}_{\nu k},\ b_{\rho k}) \in \mathbb{R}^{10}$ and include the IMU biases as well as two additional virtual biases: a velocity bias $\boldsymbol{b}_{\nu k} \in \mathbb{R}^3$ and a time bias $b_{\rho k} \in \mathbb{R}$. Define the systems' input $u_k = (\boldsymbol{w}_k,\ \boldsymbol{\tau}_k) \in \mathbb{L} \subseteq \mathbb{R}^{20}$, where $\boldsymbol{w}_k = (\boldsymbol{\omega}_k,\ \boldsymbol{a}_k,\ \boldsymbol{\nu}_k,\ \rho_k) \in \mathbb{R}^{10}$ represents the IMU readings and two additional virtual inputs: a velocity input $\boldsymbol{\nu}_k = \mathbf{0}_{3\times1}$, and a time input $\rho_k = 1$. The corresponding bias inputs are $\boldsymbol{\tau}_k = (\boldsymbol{\tau}_{\omega k},\ \boldsymbol{\tau}_{ak},\ \boldsymbol{\tau}_{\nu k},\ \tau_{\rho k}) \in \mathbb{R}^{10}$.
The resulting formulation of the noise-free IMU preintegration on the manifold $\mathcal{M}$ is presented as follows:

$$\begin{cases} \boldsymbol{\Upsilon}_{k+1} = \boldsymbol{\Upsilon}_k \exp((\boldsymbol{w}_k^\wedge - \boldsymbol{b}_k^\wedge)\delta t) \\ \boldsymbol{b}_{k+1} = \boldsymbol{b}_k + \boldsymbol{\tau}_k \delta t \end{cases}, \tag{17}$$

where $\boldsymbol{w}_k^\wedge, \boldsymbol{b}_k^\wedge \in \mathfrak{g}(3)$ and $\exp(\cdot)$ denotes the $\mathbf{G}(3)$ group exponential (6). The system written in compact form is

$$\xi_{k+1} = F_{\delta t}(\xi_k, u_k), \quad \xi_0 = (\mathbf{I}_5, \boldsymbol{b}_0), \tag{18}$$

where $F_{\delta t} : \mathcal{M} \times \mathbb{L} \to \mathcal{M}$ and

$$F_{\delta t}(\xi_k, u_k) = (\boldsymbol{\Upsilon}_k \exp((\boldsymbol{w}_k^\wedge - \boldsymbol{b}_k^\wedge)\delta t),\ \boldsymbol{b}_k + \boldsymbol{\tau}_k \delta t)\,.$$

Having successfully derived the system's evolution on the manifold, our next step is to establish the *equivalent* (*lifted*) *system* that evolves within the symmetry group. This step is crucial, as it enables us to define the *equivariant error* and to subsequently linearize its dynamics, allowing the derivation of the matrices used for the uncertainty propagation while accounting for the input measurement noise.

For the remainder of the paper we simplify the notation by defining the symmetry group $\mathbf{G}$ for the IMU preintegration problem as $\mathbf{G} \coloneqq \mathbf{G}(3) \ltimes \mathfrak{g}(3)$, that is the semi-direct product between $\mathbf{G}(3)$ and its Lie algebra [22]–[24]. Let $X_k = (C_k,\ \gamma_k) \in \mathbf{G}$ be an element of the symmetry group. Define the *state action* $\phi : \mathbf{G} \times \mathcal{M} \to \mathcal{M}$ as

$$\phi(X_k, \xi_k) \coloneqq \left(\boldsymbol{\Upsilon}_k \mathbf{C}_k,\ \mathbf{Ad}^\vee_{\mathbf{C}_k^{-1}}(\boldsymbol{b}_k - \boldsymbol{\gamma}_k^\vee)\right). \tag{19}$$

Then, ϕ is a *transitive right group action* of $\mathbf{G}$ on $\mathcal{M}$.
The inverse of the *state action* $\phi^{-1} : \mathcal{M} \times \mathcal{M} \to \mathbf{G}$ is

$$\phi^{-1}_{\mathring{\xi}}(\xi_k) = \left(\mathring{\boldsymbol{\Upsilon}}^{-1}\boldsymbol{\Upsilon}_k,\ \mathring{\boldsymbol{b}}^\wedge - (\mathbf{Ad}^\vee_{\mathring{\boldsymbol{\Upsilon}}^{-1}\boldsymbol{\Upsilon}_k}\boldsymbol{b}_k)^\wedge\right). \tag{20}$$

Define the *input action* $\psi : \mathbf{G} \times \mathbb{L} \to \mathbb{L}$ as

$$\psi(X_k, u_k) \coloneqq \left(\mathbf{Ad}^\vee_{\mathbf{C}_k^{-1}}(\boldsymbol{w}_k - \boldsymbol{\gamma}_k^\vee),\ \mathbf{Ad}^\vee_{\mathbf{C}_k^{-1}}\boldsymbol{\tau}_k\right). \tag{21}$$

Then, ψ is a *right group action* of $\mathbf{G}$ on $\mathbb{L}$. As a result, the system in (18) is *equivariant* under the actions ϕ, ψ of $\mathbf{G}$. The proof is omitted for space limitations but it follows [3]. A discrete *lift* for the system is a map $\Lambda_{\delta t} : \mathcal{M} \times \mathbb{L} \to \mathbf{G}$ with the lift condition $\phi(\Lambda_{\delta t}(\xi_k, u_k),\ \xi_k) = F_{\delta t}(\xi_k, u_k)$, $\forall \xi_k \in \mathcal{M}$ and $\forall u_k \in \mathbb{L}$ [11]. Define the discrete lift $\Lambda_{\delta t} : \mathcal{M} \times \mathbb{L} \to \mathbf{G}$ as

$$\Lambda_{\delta t}(\xi_k, u_k) \coloneqq (\Lambda_{1_{\delta t}}(\xi_k, u_k),\ \Lambda_{2_{\delta t}}(\xi_k, u_k))\,, \tag{22}$$

where

$$\begin{aligned} \Lambda_{1_{\delta t}}(\xi_k, u_k) &= \exp((\boldsymbol{w}_k^\wedge - \boldsymbol{b}_k^\wedge)\,\delta t)\,, \\ \Lambda_{2_{\delta t}}(\xi_k, u_k) &= \boldsymbol{b}_k^\wedge - \mathrm{Ad}_{\Lambda_{1_{\delta t}}(\xi_k, u_k)}\left[\boldsymbol{b}_k^\wedge + \boldsymbol{\tau}_k^\wedge \delta t\right]. \end{aligned}$$

Then, $\Lambda_{\delta t}$ is an *equivariant lift* for the system in (18) with respect to the symmetry group $\mathbf{G}$. Finally, the *lifted system* evolution on $\mathbf{G}$ is presented as follows:

$$X_{k+1} = X_k \Lambda_{\delta t}\Big(\phi_{\mathring{\xi}}(X_k), u_k\Big), \quad X_0 = \phi^{-1}_{\mathring{\xi}}(\xi_0), \tag{23}$$

where $\mathring{\xi} \in \mathcal{M}$ is an arbitrarily chosen *state origin* and the group product is defined in [22]. Note that we can transfer elements from the symmetry group $\mathbf{G}$ to the manifold $\mathcal{M}$ with $\xi_k = \phi_{\mathring{\xi}}(X_k)$, and vice versa with $X_k = \phi^{-1}_{\mathring{\xi}}(\xi_k)$.

D. Linearization of the error dynamics

The symmetry introduced in the previous subsection allows to exploit the geometric structure of the *equivariant error* [1], [2], [25] and hence to define an error as a measure between the homogeneous space and the symmetry group. Specifically, the equivariant error is defined as follows:

$$e_k \coloneqq \phi(\hat{X}_k^{-1}, \xi_k) = \left(\boldsymbol{\Upsilon}_k \hat{\mathbf{C}}_k^{-1},\ \mathbf{Ad}^\vee_{\hat{\mathbf{C}}_k}\boldsymbol{b}_k + \hat{\boldsymbol{\gamma}}_k^\vee\right), \tag{24}$$

where $\hat{X}_k = \left(\hat{C}_k,\ \hat{\gamma}_k\right) \in \mathbf{G}$ denotes the current *state estimate* on the symmetry group, and $\xi_k = (\boldsymbol{\Upsilon}_k,\ \boldsymbol{b}_k) \in \mathcal{M}$ denotes the *actual* (*true*) *state* on the manifold. Given $e_k \in \mathcal{M}$, we must define a local parametrization in the neighborhood of $\mathring{\xi}$. A typical choice of parametrization is *logarithmic* or *normal* coordinates. Let us choose normal coordinates and define a local chart $\vartheta : \mathcal{M} \to \mathbb{R}^{20}$ as

$$\vartheta(e_k) \coloneqq \log_G\Big(\phi^{-1}_{\mathring{\xi}}(e_k)\Big), \tag{25}$$

where $\log_G(\,\cdot\,) : \mathbf{G} \to \mathbb{R}^{20}$ denotes the logarithm of the tangent group $\mathbf{G}(3) \ltimes \mathfrak{g}(3)$, which is defined as follows:

$$\log_G(X_k) = \left(\log(C_k)^\vee,\ \mathbf{J}_{\mathrm{L}}(\log(C_k)^\vee)^{-1}\gamma_k^\vee\right), \tag{26}$$

with $\log(\cdot)$ and $\mathbf{J}_{\mathrm{L}}(\cdot)$ respectively denoting the $\mathbf{G}(3)$ logarithmic map (7) and the $\mathbf{G}(3)$ left jacobian matrix (8).
The error (24) expressed in local coordinates (25) is written

$$\boldsymbol{\varepsilon}_k = \vartheta(e_k) = \log_G\Big(\phi^{-1}_{\mathring{\xi}}(\phi(\hat{X}_k^{-1}, \xi_k))\Big). \tag{27}$$

By fixing $\mathring{\xi} = (\mathring{\boldsymbol{\Upsilon}},\ \mathring{\boldsymbol{b}}) = (\mathbf{I}_5,\ \mathbf{0}_{10\times1})$ and considering that

$$\hat{\xi}_k = \phi_{\mathring{\xi}}(\hat{X}_k) = (\mathring{\boldsymbol{\Upsilon}}\hat{\mathbf{C}}_k,\ \mathbf{Ad}^\vee_{\hat{\mathbf{C}}_k^{-1}}(\mathring{\boldsymbol{b}} - \hat{\boldsymbol{\gamma}}_k^\vee)) = (\hat{\boldsymbol{\Upsilon}}_k,\ \hat{\boldsymbol{b}}_k), \tag{28}$$

we can expand (27) and express it as

$$\boldsymbol{\varepsilon}_k = \left(\log(\boldsymbol{\Upsilon}_k\hat{\boldsymbol{\Upsilon}}_k^{-1})^\vee,\ -\mathbf{J}_{\mathrm{L}}(\log(\boldsymbol{\Upsilon}_k\hat{\boldsymbol{\Upsilon}}_k^{-1})^\vee)^{-1}\mathbf{Ad}^\vee_{\boldsymbol{\Upsilon}_k}(\boldsymbol{b}_k - \hat{\boldsymbol{b}}_k)\right). \tag{29}$$

Let us consider a *noisy* input $\tilde{u}_k = (\tilde{\boldsymbol{w}}_k,\ \tilde{\boldsymbol{\tau}}_k)$. $\tilde{\boldsymbol{w}}_k = \boldsymbol{w}_k + \boldsymbol{\eta}_{wk}$ includes the noisy and biased IMU measurements $\tilde{\boldsymbol{\omega}}_k$ and $\tilde{\boldsymbol{a}}_k$ as well as the two virtual inputs $\boldsymbol{\nu}_k$ and ρ_k introduced in Sec. III-C. $\tilde{\boldsymbol{\tau}}_k = \boldsymbol{\tau}_k + \boldsymbol{\eta}_{\tau k}$ denotes the noisy bias input. The

Table I
IMU PREINTEGRATION COMPARISON: NEES MEDIAN FOR DIFFERENT PREINTEGRATION TIMES Δt_{ij} ON THE EUROC MAV DATASET [20].

Method	$\mathbf{SO}(3)\times\mathbb{R}^6\times\mathbb{R}^6$ [13]			LI-$\mathbf{SE}_2(3)\times\mathbb{R}^6$ [16]			RI-$\mathbf{SE}_2(3)\times\mathbb{R}^6$ [17]			MAVIS [18]			$\mathbf{G}(3)\ltimes\mathfrak{g}(3)$		
Δt_{ij}	$0.2s$	$0.5s$	$1.0s$	$0.2s$	$0.5s$	$1.0s$	$0.2s$	$0.5s$	$1.0s$	$0.2s$	$0.5s$	$1.0s$	$0.2s$	$0.5s$	$1.0s$
MH_01	1.374	2.547	4.070	1.374	2.545	4.070	1.373	2.545	4.071	1.371	2.549	4.030	**1.186**	**1.866**	**2.347**
MH_02	1.113	2.077	2.871	1.113	2.077	2.871	1.114	2.078	2.870	1.096	2.071	2.867	**0.946**	**1.526**	**1.755**
MH_03	1.210	2.667	4.545	1.208	2.663	4.545	1.215	2.660	4.547	1.219	2.660	4.537	**1.207**	**2.269**	**3.221**
MH_04	1.222	2.638	4.506	1.216	2.641	4.534	1.220	2.635	4.531	1.220	2.636	4.524	**1.204**	**2.469**	**2.757**
MH_05	1.383	3.404	4.516	1.383	3.405	4.502	1.383	3.405	4.515	1.382	3.378	4.512	**1.377**	**2.645**	**2.668**
V1_01	1.741	5.139	10.141	1.741	5.145	10.133	1.744	5.147	10.149	1.741	5.151	10.130	**1.716**	**4.837**	**8.302**
V1_02	1.363	2.456	3.844	1.370	2.466	3.834	1.371	2.463	3.837	1.382	2.467	3.841	**1.339**	**2.330**	**2.458**
V1_03	1.828	3.783	5.891	1.793	3.816	5.856	1.789	3.824	5.800	1.830	3.801	6.007	**1.734**	**3.331**	**3.457**
V2_01	2.024	5.644	8.406	2.023	5.643	8.411	2.022	5.649	8.413	2.024	5.644	8.402	**2.006**	**5.350**	**7.342**
V2_02	2.579	6.627	9.788	2.574	6.620	9.573	2.579	6.627	9.761	2.576	6.634	9.732	**2.573**	**6.430**	**8.422**
V2_03	3.047	8.290	13.549	3.047	8.216	13.573	3.047	8.213	13.546	3.047	8.254	13.623	**3.025**	**7.935**	**11.145**

The **best** results are in bold and the second-best results are underlined.

linearized error dynamics about $\boldsymbol{\varepsilon}_k = \mathbf{0} \in \mathbb{R}^{20}$ is then derived as follows:

$$\boldsymbol{\varepsilon}_{k+1} \approx \hat{\mathbf{A}}_{k+1}\,\boldsymbol{\varepsilon}_k + \hat{\mathbf{B}}_{k+1}\,\boldsymbol{\eta}_k \tag{30}$$

with $\boldsymbol{\eta}_k = (\boldsymbol{\eta}_{wk},\ \boldsymbol{\eta}_{\tau k}) \in \mathbb{R}^{20}$,

$$\hat{\mathbf{A}}_{k+1} = \begin{bmatrix} \mathbf{I}_{10} & \mathbf{J}_{\mathrm{L}}(\mathring{\boldsymbol{w}}_k\delta t)\delta t \\ \mathbf{0}_{10\times 10} & \mathbf{Ad}^{\vee}_{\exp(\mathring{\boldsymbol{w}}_k^{\wedge}\delta t)} \end{bmatrix}, \tag{31}$$

$$\hat{\mathbf{B}}_{k+1} = \begin{bmatrix} -\mathbf{Ad}^{\vee}_{\hat{\boldsymbol{\Upsilon}}_k}\mathbf{J}_{\mathrm{L}}((\tilde{\boldsymbol{w}}_k - \hat{\boldsymbol{b}}_k)\delta t)\delta t & \mathbf{0}_{10\times 10} \\ \mathbf{0}_{10\times 10} & -\mathbf{Ad}^{\vee}_{\hat{\boldsymbol{\Upsilon}}_{k+1}}\delta t \end{bmatrix}, \tag{32}$$

and $\mathring{u}_k \coloneqq \psi(\hat{X}_k^{-1}, \tilde{u}_k) = (\mathring{\boldsymbol{w}}_k,\ \mathring{\boldsymbol{\tau}}_k) \Rightarrow \mathring{\boldsymbol{w}}_k = \mathbf{Ad}^{\vee}_{\hat{\boldsymbol{\Upsilon}}_k}(\tilde{\boldsymbol{w}}_k - \hat{\boldsymbol{b}}_k)$.

E. Bias update and practical implementation

From (17) we note that the preintegration matrix $\hat{\boldsymbol{\Upsilon}}_{k+1}$ is recursively calculated using the current bias estimate during the mean propagation. Since it would be very time-consuming to repeat the whole computation every time the estimated bias gets updated during the optimization process, we perform the *bias update* using first-order approximation similarly to [17]. The Jacobian matrix of ξ_{k+1} with respect to $\hat{\boldsymbol{b}}_k$ is propagated iteratively as $\mathbf{J}_{\xi_{k+1}} = \boldsymbol{\Phi}_{\mathbf{b}k+1}\mathbf{J}_{\xi_k}$ starting from $\mathbf{J}_{\xi_0} = \mathbf{I}_{20}$, with

$$\boldsymbol{\Phi}_{\mathbf{b}k+1} = \begin{bmatrix} \mathbf{I}_{10} & -\mathbf{Ad}^{\vee}_{\hat{\boldsymbol{\Upsilon}}_k}\mathbf{J}_{\mathrm{L}}((\tilde{\boldsymbol{w}}_k - \hat{\boldsymbol{b}}_k)\delta t)\delta t \\ \mathbf{0}_{10\times 10} & \mathbf{I}_{10} \end{bmatrix}. \tag{33}$$

Then, given a new bias estimate $\hat{\boldsymbol{b}}_0^{+} \leftarrow \hat{\boldsymbol{b}}_0 + \Delta\hat{\boldsymbol{b}}$, the bias update on the preintegration matrix is performed as

$$\hat{\boldsymbol{\Upsilon}}_{k+1}^{+} \approx \exp((\mathbf{J}_{\boldsymbol{\Upsilon}k+1}\Delta\hat{\boldsymbol{b}})^{\wedge})\hat{\boldsymbol{\Upsilon}}_{k+1}, \tag{34}$$

where $\mathbf{J}_{\boldsymbol{\Upsilon}k+1} \in \mathbb{R}^{10\times 10}$ is the upper right 10×10 corner of $\mathbf{J}_{\xi_{k+1}}$, and $\exp(\cdot)$ is the $\mathbf{G}(3)$ exponential map (6).

We finally derived all the necessary components for our novel *equivariant* IMU preintegration, summarized in Alg. 1, which iteratively propagates both mean $\hat{X}_k$ and covariance $\boldsymbol{\Sigma}_k$ of the equivariant error, together with the Jacobian $\mathbf{J}_{\xi_k}$ for the bias update. To streamline C++ development, we added both $\mathbf{G}(3)$ and its tangent group $\mathbf{G}(3)\ltimes\mathfrak{g}(3)$ to the header-only open-source library Lie++[2].

IV. EXPERIMENTS AND RESULTS

To assess the real-world performance of our novel *equivariant* IMU preintegration on $\mathbf{G}(3)\ltimes\mathfrak{g}(3)$, we selected the well-known and widely recognized EuRoC MAV dataset [20], which provides ground-truth poses, velocities and IMU biases, as well as IMU measurements and noise parameters. We partitioned each dataset sequence into sub-trajectories with a duration corresponding to a preintegration time Δt_{ij}. We then performed the IMU preintegration for each sub-sequence with different methods, starting from the ground-truth values and with the same initial covariance, and we computed the NEES at the end of Δt_{ij}. This process was iterated across various preintegration times, and we analyzed the NEES distribution over all sub-sequences to derive statistical information for each method. The proposed approach outperforms state-of-the-art methods [13], [16]–[18] in terms of consistency across all sequences in the dataset, as reported in Tab. I.

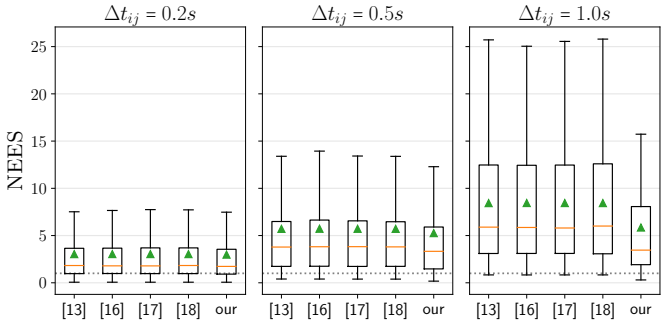

Figure 1. Consistency comparison on the EuRoC MAV dataset [20]: NEES box-plot for different preintegration times $\Delta t_{ij} = [0.2s,\ 0.5s,\ 1.0s]$ on the V1_03 sequence. Orange lines indicate the medians while green triangles denote the means.

V. CONCLUSION

This paper introduces a theoretical framework for IMU preintegration on $\mathbf{G}(3)\ltimes\mathfrak{g}(3)$ and successfully demonstrates its performance when compared with state-of-the-art methodologies. Specifically, in this work, we leverage the tangent group symmetry of the inhomogeneous Galilean group $\mathbf{G}(3)$ to define a novel preintegration error that geometrically couples the navigation states and the bias states, ultimately improving the covariance propagation, and hence the consistency, for the preintegrated IMU measurements. Results show that the proposed approach achieves the best NEES in every sequence of the EuRoC MAV dataset and for every preintegration time. Future work will focus on implementing and evaluating the proposed preintegration method in a factor graph-based state estimator.

[2]https://github.com/aau-cns/Lie-plusplus

REFERENCES

[1] P. Van Goor, T. Hamel, and R. Mahony, "Equivariant Filter (EqF): A General Filter Design for Systems on Homogeneous Spaces," *Proceedings of the IEEE Conference on Decision and Control*, vol. 2020-Decem, no. Cdc, pp. 5401–5408, 2020.

[2] P. van Goor, T. Hamel, and R. Mahony, "Equivariant Filter (EqF)," *IEEE Transactions on Automatic Control*, vol. 68, no. 6, pp. 3501 – 3512, 6 2022.

[3] A. Fornasier, Y. Ng, R. Mahony, and S. Weiss, "Equivariant Filter Design for Inertial Navigation Systems with Input Measurement Biases," *2022 International Conference on Robotics and Automation (ICRA)*, pp. 4333–4339, 5 2022.

[4] A. Fornasier, Y. Ge, P. van Goor, R. Mahony, and S. Weiss, "Equivariant Symmetries for Inertial Navigation Systems," *arXiv preprint arXiv:2309.03765*, 9 2023.

[5] P. van Goor and R. Mahony, "An Equivariant Filter for Visual Inertial Odometry," *Proceedings - IEEE International Conference on Robotics and Automation*, vol. 2021-May, pp. 1875–1881, 2021.

[6] P. Van Goor and R. Mahony, "EqVIO: An Equivariant Filter for Visual-Inertial Odometry," *IEEE Transactions on Robotics*, vol. 39, no. 5, pp. 3567–3585, 10 2023.

[7] T. Bouazza, K. Ashton, P. Van Goor, R. Mahony, and T. Hamel, "Equivariant Filter for Feature-Based Homography Estimation for General Camera Motion," *Proceedings of the IEEE Conference on Decision and Control*, pp. 8463–8470, 2023.

[8] A. Fornasier, Y. Ng, C. Brommer, C. Bohm, R. Mahony, and S. Weiss, "Overcoming Bias: Equivariant Filter Design for Biased Attitude Estimation With Online Calibration," *IEEE Robotics and Automation Letters*, vol. 7, no. 4, pp. 12 118–12 125, 10 2022.

[9] M. Scheiber, A. Fornasier, C. Brommer, and S. Weiss, "Revisiting Multi-GNSS Navigation for UAVs – An Equivariant Filtering Approach," *2023 21st International Conference on Advanced Robotics (ICAR)*, pp. 134–141, 12 2023.

[10] A. Fornasier, P. v. Goor, E. Allak, R. Mahony, and S. Weiss, "MSCEqF: A Multi State Constraint Equivariant Filter for Vision-aided Inertial Navigation," *IEEE Robotics and Automation Letters*, 1 2023.

[11] Y. Ge, P. Van Goor, and R. Mahony, "Equivariant Filter Design for Discrete-time Systems," *Proceedings of the IEEE Conference on Decision and Control*, vol. 2022-December, pp. 1243–1250, 2022.

[12] A. Barrau and S. Bonnabel, "The Invariant Extended Kalman Filter as a Stable Observer," *IEEE Transactions on Automatic Control*, vol. 62, no. 4, pp. 1797–1812, 2017.

[13] C. Forster, L. Carlone, F. Dellaert, and D. Scaramuzza, "On-Manifold Preintegration for Real-Time Visual-Inertial Odometry," *IEEE Transactions on Robotics*, vol. 33, no. 1, pp. 1–21, 2 2017.

[14] K. Eckenhoff, P. Geneva, and G. Huang, "Closed-form preintegration methods for graph-based visual–inertial navigation," *The International Journal of Robotics Research*, vol. 38, no. 5, pp. 563–586, 2019.

[15] Y. Yang, B. P. Wisely Babu, C. Chen, G. Huang, and L. Ren, "Analytic Combined IMU Integration (ACI2) For Visual Inertial Navigation," in *2020 IEEE International Conference on Robotics and Automation (ICRA)*, 2020, pp. 4680–4686.

[16] M. Brossard, A. Barrau, P. Chauchat, and S. Bonnabel, "Associating Uncertainty to Extended Poses for on Lie Group IMU Preintegration With Rotating Earth," *IEEE Transactions on Robotics*, vol. 38, no. 2, pp. 998–1015, 2021.

[17] S.-H. Tsao and S.-S. Jan, "Analytic IMU Preintegration That Associates Uncertainty on Matrix Lie Groups for Consistent Visual–Inertial Navigation Systems," *IEEE Robotics and Automation Letters*, vol. 8, no. 6, pp. 3820–3827, 2023.

[18] Y. Wang, Y. Ng, I. Sa, A. Parra, C. Rodriguez, T. J. Lin, and H. Li, "MAVIS: Multi-Camera Augmented Visual-Inertial SLAM using SE2(3) Based Exact IMU Pre-integration," 2 2023.

[19] M. Fourmy, D. Atchuthan, N. Mansard, J. Sola, and T. Flayols, "Absolute humanoid localization and mapping based on IMU Lie group and fiducial markers," *IEEE-RAS International Conference on Humanoid Robots*, vol. 2019-October, pp. 237–243, 10 2019.

[20] M. Burri, J. Nikolic, P. Gohl, T. Schneider, J. Rehder, S. Omari, M. W. Achtelik, and R. Siegwart, "The EuRoC micro aerial vehicle datasets," *https://doi.org/10.1177/0278364915620033*, vol. 35, no. 10, pp. 1157–1163, 1 2016.

[21] M. Bloesch, M. Hutter, M. Hoepflinger, S. Leutenegger, C. Gehring, C. David Remy, and R. Siegwart, "State Estimation for Legged Robots - Consistent Fusion of Leg Kinematics and," *Robotics: Science and Systems VIII*, 7 2012.

[22] Y. Ng, P. Van Goor, R. Mahony, and T. Hamel, "Attitude Observation for Second Order Attitude Kinematics," in *Proceedings of the IEEE Conference on Decision and Control*, vol. 2019-Decem. IEEE, 2019, pp. 2536–2542.

[23] Y. Ng, P. Van Goor, T. Hamel, and R. Mahony, "Equivariant Systems Theory and Observer Design for Second Order Kinematic Systems on Matrix Lie Groups," *Proceedings of the IEEE Conference on Decision and Control*, vol. 2020-Decem, no. Xx, pp. 4194–4199, 2020.

[24] Y. Ng, P. van Goor, and R. Mahony, "Pose Observation for Second Order Pose Kinematics," *IFAC-PapersOnLine*, vol. 53, no. 2, pp. 2317–2323, 1 2020.

[25] R. Mahony, P. Van Goor, and T. Hamel, "Observer Design for Nonlinear Systems with Equivariance," *https://doi.org/10.1146/annurev-control-061520-010324*, vol. 5, pp. 221–252, 5 2022.